

# Morphologically bioinspired hierarchical Nylon 6,6 electrospun assembly recreating the structure and performance of tendons and ligaments

Alberto Sensini<sup>1</sup>, Carlo Gotti<sup>1</sup>, Juri Belcari<sup>1</sup>, Andrea Zucchelli<sup>1</sup>,  
Maria Letizia Focarete<sup>2,3</sup>, Chiara Gualandi<sup>2,4</sup>, Ivan Todaro<sup>1</sup>, Alexander P. Kao<sup>5</sup>,  
Gianluca Tozzi<sup>5</sup>, Luca Cristofolini<sup>1,3</sup>

- <sup>1</sup> Department of Industrial Engineering, Alma Mater Studiorum—University of Bologna, I-40131 Bologna, Italy
- <sup>2</sup> Department of Chemistry ‘G. Ciamician’ and National Consortium of Materials Science and Technology (INSTM, Bologna RU), Alma Mater Studiorum—University of Bologna, I-40126 Bologna, Italy
- <sup>3</sup> Health Sciences and Technologies—Interdepartmental Center for Industrial Research (CIRI-HST), Alma Mater Studiorum—University of Bologna, I-40064 Ozzano dell’Emilia, Bologna, Italy
- <sup>4</sup> Advanced Mechanics and Materials – Interdepartmental Center for Industrial Research (CIRI-MAM), Alma Mater Studiorum—University of Bologna, I-40123 Bologna, Italy
- <sup>5</sup> Zeiss Global Centre, School of Mechanical and Design Engineering, University of Portsmouth, Portsmouth PO1 3DJ, United Kingdom

**Submitted to: Medical Engineering & Physics – Special Issue on Biofabrication**

**Version.0:** 1<sup>st</sup> February 2019

**Version.1:** 17<sup>th</sup> May 2019

**Statistics:**

Word count (manuscript):	5023 (Introduction through acknowledgements, excluding references, captions and tables)
Word count (abstract):	248 words
Figures:	9
Tables:	1
References:	58

**Corresponding author:**

Luca Cristofolini  
Department of Industrial Engineering  
Alma Mater Studiorum – Università di Bologna  
Via Umberto Terracini 28  
40131 Bologna, Italy  
e-mail: [luca.cristofolini@unibo.it](mailto:luca.cristofolini@unibo.it)

1 **Abstract**

2 Reconstructions of ruptured tendons and ligaments currently have dissatisfactory failure  
3 rate. Failures are mainly due to the mechanical mismatch of commercial implants with  
4 respect to the host tissue. In fact, it is crucial to replicate the morphology (hierarchical  
5 in nature) and mechanical response (highly-nonlinear) of natural tendons and ligaments.  
6 The aim of this study was to develop morphologically bioinspired hierarchical Nylon  
7 6,6 electrospun assemblies recreating the structure and performance of tendons and  
8 ligaments. First, we built different electrospun bundles to find the optimal orientation  
9 of the nanofibers. A 2nd-level hierarchical assembly was fabricated with a dedicated  
10 process that allowed tightly joining the bundles one next to the other with an electrospun  
11 sheath, so as to improve the mechanical performance. Finally, a further hierarchical 3rd-  
12 level assembly was constructed by grouping several 2nd-level assemblies. The  
13 morphology of the different structures was assessed with scanning electron microscopy  
14 and high-resolution X-ray tomography, which allowed measuring the directionality of  
15 the nanofibers in the bundles and in the sheaths. The mechanical properties of the single  
16 bundles and of the 2nd-level assemblies were measured with tensile tests. The single  
17 bundles and the hierarchical assemblies showed morphology and directionality of the  
18 nanofibers similar to the tendons and ligaments. The strength and stiffness were  
19 comparable to that of tendons and ligaments. In conclusion, this work showed an  
20 innovative electrospinning production process to build nanofibrous Nylon 6,6  
21 hierarchical assemblies which are suitable as future implantable devices and able to  
22 mimic the multiscale morphology and the biomechanical properties of tendons and  
23 ligaments.

24 **Keywords:** Bioinspired Structures; Electrospinning; Hierarchical Devices; Tendons and  
25 Ligaments  
26

27 **1. Introduction**

28 The design and development of innovative solutions to repair or substitute injured  
29 tendons and ligaments is one of extreme interest in orthopaedic research. In fact,  
30 approximately 30 million new cases of tendon and ligament injuries are diagnosed  
31 worldwide annually [1]. From over 33 million musculoskeletal injuries per year in the  
32 United States alone, almost 50% of them are tendon and ligament related, with about  
33 95,000 new cases annually [2]. The difficulty in healing these tissues is mainly related  
34 to their non-linear mechanical properties and complex hierarchical structure, composed  
35 of collagen fibers that are axially aligned and organized in different levels of aggregation  
36 [3–5]. Above all, due to low cellular activity, the injuries of elderly people generally  
37 require the use of permanent inert prosthetic devices [6–8]. An inert polymeric material  
38 frequently used for devices in this field is Nylon 6,6, which has been approved as an  
39 implantable material [9]. For instance, Nylon 6,6 is found in commercially available  
40 suture wires [10,11] and tendon grafts [12].

41 The most popular examples of inert devices for tendon and ligament are Lars<sup>®</sup> Ligament,  
42 Leeds-Keio<sup>®</sup> (i.e. Poly-tape<sup>®</sup>) and Gore-Tex<sup>®</sup> [12]. In the last two decades, several  
43 studies published in literature have assessed the clinical quality of these devices [8].  
44 However, even if they have adequate mechanical behavior, compared to the native  
45 tendon or ligament tissue, they have a different morphology and are not hierarchically  
46 structured. The Lars<sup>®</sup> Ligament is composed of aligned microfibers grouped together  
47 by an external knitted membrane; Leeds-Keio<sup>®</sup> (i.e. Poly-tape<sup>®</sup>) is a totally  
48 knitted/waved microfibrous device; while Gore-Tex<sup>®</sup> is made of groups of aligned  
49 microfibers braided together to obtain the final device. However, all these textile  
50 patterns produce implantable devices have a very different morphology when compared  
51 to a natural tendon or ligament [13]. In fact, tendon or ligament tissue is composed of  
52 collagen nanofibers preferentially axially aligned, organized in different levels of  
53 aggregation and covered by membranes of randomly arranged collagen nanofibers

54 [3,4,14]. The lack of bioinspired hierarchical organization of these implantable devices,  
55 can often cause inflammatory outcomes and post-operative complications [8,12].  
56 Furthermore, several clinical follow-ups of such devices have shown controversial  
57 outcomes, in terms of failure or success over a long-term period [8]. Among the others,  
58 Lars<sup>®</sup> Ligament showed the most promising results for long term positive outcomes of  
59 the implants and low incidence of revision surgery in Anterior Cruciate Ligament (ACL)  
60 applications [15]. However minor episodes of knee stiffness and synovitis were  
61 documented in the past [8,15,16]. The published studies about the clinical performances  
62 in ACL reconstruction using the Leeds-Keio<sup>®</sup>, despite several positive results, showed  
63 frequent events of re-rupture, tunnel enlargement, synovitis associated with polyester  
64 particles, greater pivot-shift and laxity, especially until the early 2000s [17–20].  
65 Moreover different applications of this device were explored to repair other tendons and  
66 ligaments such as rotator cuff, knee extensor, Achilles tendon, iliofemoral ligament and  
67 ankle lateral ligament [8]. Gore-Tex<sup>®</sup> devices showed satisfactory results to treat very  
68 large rotator cuff tears and patellar reconstructions [21,22], but due to severe osteolytic  
69 complications were completely abandoned for ACL applications [8,23,24].  
70 A promising approach to overcome the morphological and mechanical limitations of  
71 these devices is offered by the electrospinning technology. Producing polymeric  
72 nanofibers by stretching solutions in high electrostatic fields, the electrospinning  
73 technique has demonstrated the ability to fabricate scaffolds that mimic the tendon and  
74 ligament tissue [25,26]. However, to date no one has used electrospinning to produce  
75 complex assemblies that reproduce the hierarchical structure and mechanical properties  
76 of a whole tendon or ligament [27].  
77 The aim of this study was to develop morphologically bioinspired hierarchical  
78 assemblies (made of inert Nylon 6,6) to replicate the biomechanical response of natural  
79 tendon and ligament. For this reason, three levels of aggregation were investigated: (i)  
80 bundles of random and aligned electrospun nanofibers; (ii) a 2nd-level hierarchical

81 assembly built using the most promising type of bundles (aligned nanofibers); (iii) a 3rd-  
82 level hierarchical assembly containing several 2nd-levels hierarchical assemblies. For  
83 all of these structures, the morphology and the associated mechanical properties were  
84 investigated.  
85

## 86 **2. Materials and methods**

87 In order to develop a complex hierarchical structure, in the first phase two different  
88 methods for producing electrospun bundles were developed: in one instance, the  
89 nanofibers were randomly aligned, while in the second instance a high alignment of the  
90 nanofibers was achieved. The morphology of the Bundles was characterized with  
91 Scanning Electron Microscopy (SEM) and High-Resolution X-ray Computed  
92 Tomography (XCT); mechanical tests were performed to assess the strength and  
93 modulus of elasticity of the constructs. The most promising candidates (bundles of  
94 aligned nanofibers) were used to produce the 2nd-level hierarchical assemblies, which  
95 were again characterized in terms of morphology and mechanical properties. The 3rd-  
96 level hierarchical assembly was built by joining three 2nd-level hierarchical assemblies,  
97 and its morphology was fully characterized.

### 98 *2.1. Materials*

99 Nylon 6,6 pellets, kindly provided by DuPont (Wilmington, USA), were dissolved in a  
100 trifluoroacetic acid (TFA) (Carlo Erba, Milan, Italy) and acetone (AC) (Sigma Aldrich,  
101 Saint-Louis, USA) mixture, in order to obtain the following solution: 15% (w/v) solution  
102 of Nylon 6,6 dissolved in TFA:AC = 50:50 (v/v).

### 103 *2.2. Identification of optimal electrospun bundle preparation*

#### 104 *2.2.1. Electrospun bundles production*

105 Electrospun bundles were produced using a laboratory electrospinning machine  
106 (Spinbow Lab Unit, Spinbow S.r.l., Bologna, Italy), equipped with a linear sliding  
107 spinneret (carrying four syringes ejecting the same polymeric solution) and a rotating

108 drum collector (diameter = 150 mm; length = 500 mm). A syringe pump (KD Scientific  
109 200 series, Illinois, USA) and four glass syringes were used to electrospin the solution.  
110 Each syringe was connected to a stainless-steel blunt-ended needle (inner diameter =  
111 0.84 mm) with a PTFE tube. The electrospinning was performed at room temperature  
112 (RT) and relative humidity 20-30%. The solution was electrospun with an applied  
113 voltage of 20 kV and a feed rate of 0.50 mL h<sup>-1</sup>. The drum collector was positioned 160  
114 mm away from the needle tips. The sliding spinneret with the four needles had an  
115 excursion of 100 mm, with a sliding speed of 1200 mm min<sup>-1</sup>. The mats of nanofibers  
116 were cut circumferentially into strips.

117 In order to reach the best configuration in terms of fiber orientation and mechanical  
118 properties, different electrospun bundles were produced. Bundles made of random  
119 fibers were obtained by rotating the drum collector with a low peripheral speed of 0.78  
120 m s<sup>-1</sup> and for an electrospinning time of 1.5 hours (Fig. 1). The mats of random  
121 nanofibers were cut into 70 mm wide strips, and manually wrapped to produce bundles,  
122 with a cross-sectional diameter of approximately 550-650 micrometers. At the end of  
123 the procedure, the bundles (about 470 mm in length) were cut in an extremity and  
124 removed from the collector (Fig. 1).

125 However, in order to improve the mechanical properties of the random bundles (see  
126 results section), bundles of aligned nanofibers were produced. To obtain mats of  
127 nanofibers preferentially aligned in the direction of drum rotation, the drum collector  
128 was rotated with a higher peripheral speed of 22.8 m s<sup>-1</sup> during an electrospinning time  
129 of 3 hours. The mats of aligned nanofibers were cut into 50 mm wide strips, and rolled  
130 on the drum as previously described.

131

132 2.2.2. *Morphological investigation of bundles*

133 To examine the surface morphology of the Nylon 6,6 bundles, Scanning Electron  
134 Microscopy (SEM) analysis was performed. A commercial SEM (Philips 515 SEM,  
135 Amsterdam, Netherlands) was used with a voltage of 15 kV, on samples sputter-coated  
136 with gold. The diameter of the nanofibers and their distribution (mean and SD) were  
137 measured on the SEM images of 200 fibers, by means of the image analysis software  
138 ImageJ [28].

139 To measure the mean diameter of each bundle a light optical microscope (Axioskop,  
140 Zeiss, Pleasanton, CA, USA) equipped with a camera (AxioCam MRc, Zeiss,  
141 Pleasanton, CA, USA) was used and image analysis was performed using ImageJ [28].  
142 For each bundle, the mean and standard deviation (SD) of ten measurements was  
143 computed. To measure the weight of each specimen a precision balance was used (MC  
144 210 P, capacity resolution: 210 g x 0.01 mg, Sartorius, Göttingen, Germany). For each  
145 bundle, the mean and SD of three measurements was computed.

146 In order to investigate the three-dimensional structure of the Nylon 6,6 bundles, high-  
147 resolution x-ray tomographic scans were acquired with a laboratory XCT (Versa 510,  
148 Zeiss, Pleasanton, CA, USA). For the XCT scans, the following settings were used: 40  
149 kV Voltage, 3 W Power, 75.5 microAmpere tube current. Projections were collected at  
150 rotational steps of  $0.18^\circ$  over  $360^\circ$ , with a voxel size 0.4 micrometers, using 14 second  
151 exposure time (scanning time of approximately 10 hours).

152 All the XCT images, were reconstructed using the Scout-and-Scan Reconstructor  
153 software (Zeiss), and were visualized using XM3DViewer1.2.8 software (Zeiss).

154



155 *2.2.3. Directionality of the nanofibers in the bundles*

156 In order to quantify the distribution of orientation of the nanofibers in the bundles, the  
157 Directionality plugin of ImageJ was used [28–30]. This approach allowed to quantify  
158 the amount of nanofibers within a given angle from the axis. The analysis was  
159 performed using a Local Gradient Orientation method following a procedure previously  
160 validated [31]. For the random nanofiber bundles the Directionality analysis was  
161 performed on stacks of five SEM images (magnification = 8000x). For the aligned  
162 nanofiber bundle a full volume investigation was performed applying the same  
163 procedure to all the slices of the XCT stacks, after reslicing.

164 *2.2.4. Mechanical characterization of the bundles*

165 The mechanical properties of the random and aligned nanofiber bundles were measured  
166 with a servo-hydraulic testing machine (8032, Instron, High Wycombe, UK), with a  $\pm 1$   
167 kN dynamic cell (Instron, High Wycombe, UK). The force signals had a noise of 0.01  
168 N after filtering. All the specimens were immersed in saline for two minutes before the  
169 mechanical test. The test machine was operated in displacement control, adjusting the  
170 actuator speed according to the actual specimen length, to obtain a strain rate of  $70\% \text{ s}^{-1}$ .  
171 This strain rate is in the range of those experienced by tendons and ligaments during  
172 strenuous physiological activities [32–35].

173 Ten specimens of both random and aligned nanofiber bundles were tested. Dedicated  
174 capstan grips (Fig. 5) were used to minimize the stress concentration at the specimens  
175 ends. The gauge length was 47.42 mm (this included the free length and the portion of  
176 specimen wrapped around the capstans, consistent with the BS EN 12562:1999 and the  
177 ASTM D2256/D2256M-10 (2015) Standards).

178 The mechanical characterization of the random and aligned bundles was performed to  
179 identify the most biomimetic candidate, so just the typical load-strain curves and the  
180 force and stress data were analyzed (see 2.3.4 section and Fig. 2).

### 181 *2.3. Optimization of the hierarchical assemblies*

182 Based on the most promising configuration from section 2.2 (see Results), aligned  
183 bundles were adopted for the following steps. In order to allow easier handling and  
184 stretching of the bundles in the subsequent steps of preparation of the hierarchical  
185 structures, the bundles were removed from the collector without any cut, thus obtaining  
186 ring-shaped bundles (Fig. 1).

#### 187 *2.3.1. Fabrication of the hierarchical assemblies*

188 In order to reproduce the whole morphology of a tendon or ligament [4,14,27], two  
189 different electrospun bioinspired assembly were produced.

190 To group together different numbers of bundles, an innovative electrospinning  
191 procedure to electrospin nanofibrous sheaths was developed (Fig. 1). These sheath were  
192 designed to reproduce the morphology of the natural membranes of tendons (endotenon,  
193 epitenon) or ligaments (endoligament, epiligament) [4,27]. The same electrospinning  
194 parameters previously described were used.

195 Two custom made stainless-steel 6-arms capstan grips (6 cylindrical arms of 8 mm of  
196 diameter each) were fixed in a custom-made rotating electrospinning machine. Then,  
197 24 bundles were hooked on the grips, 4 for each arm (Fig. 1). After this operation, a  
198 Nylon 6,6 sheath of nanofibers was electrospun on the group of bundles for 12 hours.  
199 The custom-made electrospinning apparatus was composed of a high-voltage power  
200 supply (FuG Elektronik GmbH, Schechen, Germany), two syringe pumps (KD

201 Scientific Legato 100, Illinois, USA), and two glass syringes containing the polymeric  
202 solution, connected to stainless-steel blunt-ended needles (inner diameter = 0.84 mm)  
203 by PTFE tubes.

204 In order to concentrate the nanofibers on the group of bundles, a flat aluminum collector  
205 plate (200 mm high and 50 mm wide) was placed behind the bundles (Fig. 1). To pre-  
206 strain the nanofibers of the sheath on the final assembly surface, the group of bundles  
207 was in a static position, and intermittently put in rotation (approximately 20 rpm for 1  
208 minute every 5 minutes), while the sheath was being electrospun (Fig. 1).

209 Finally, in order to produce a hierarchical assembly to completely simulate the structure  
210 of a whole tendon or ligament [4,27], including the endotenon/endoligament sheaths and  
211 the tertiary fiber bundles inside, a 3rd-level hierarchical assembly was produced. First,  
212 three Nylon 6,6 2nd-level hierarchical assemblies, with five ring-shaped bundles each,  
213 were produced as previously described (with an electrospinning session of 10 hours  
214 each). Then, the extremities of the three 2nd-level hierarchical assemblies were tied  
215 together with paper tape, and fixed in the machine (Fig.1). To produce the  
216 epitenon/epiligament-like sheath, the same procedure and methods previously described  
217 were used, with an electrospinning session of 10 hours (Fig. 1).

### 218 *2.3.2. Morphological investigation of the hierarchical assemblies*

219 The SEM and light optical microscope investigations on the 2nd-level and 3rd-level  
220 hierarchical assemblies were performed with the same parameters previously described  
221 in section 2.2.2.

222 To investigate the three-dimensional structure of the Nylon 6,6 hierarchical assemblies,  
223 the XCT scans were acquired with a different high-resolution x-ray tomography system  
224 (Versa 520, Zeiss, Pleasanton, CA, USA). The following parameters were used

225 (depending on the shape and thickness of the specimens): (i) 2nd-level hierarchical  
226 assembly: 50 kV Voltage, 4 W Power, 80 microAmpere tube current, 5.27 micrometers  
227 voxel size, 1.75 second exposure time, rotational steps of  $0.12^\circ$  over  $360^\circ$ , for a scanning  
228 time of 7.5 hours; (ii) 3rd-level hierarchical assembly: 50 kV Voltage, 3 W Power, 60  
229 microAmpere tube current, 5.27 micrometers voxel size, 1.75 second exposure time,  
230 rotational steps of  $0.12^\circ$  over  $360^\circ$ , for a scanning time of 7.5 hours.

231 All the XCT images, were reconstructed using the Scout-and-Scan Reconstructor  
232 software (Zeiss), and were visualized using XM3DViewer1.2.8 software (Zeiss).

### 233 *2.3.3. Directionality of the nanofibers of the sheath and of the internal bundles*

234 In order to quantify the orientation of the nanofibers in the electrospun sheaths and in  
235 the bundles inside the assemblies, the Directionality plugin of ImageJ was used [28–30],  
236 as described above in the bundles section. The Directionality analysis was performed  
237 with two different approaches derived from Sensini et al. [31].

238 For the external sheaths, the Directionality analysis was performed on stacks of 5 SEM  
239 surface images (magnification = 8000x). To assess the orientation of the bundles inside  
240 the hierarchical assemblies, a full volume investigation was performed applying the  
241 procedure to all the slices of the XCT stacks, after a reslice.

### 242 *2.3.4. Mechanical characterization of the hierarchical assemblies*

243 The mechanical characterization was performed both on the ring-shaped bundles and on  
244 the 2nd-level hierarchical assemblies (due to limited availability of specimens, the  
245 mechanical tests were not performed on the 3rd-level hierarchical assembly).

246 As the hierarchical assemblies were built with ring-shaped bundles (as opposed to the  
247 straight bundles tested before, see 2.2.4) the mechanical test was performed starting from

248 the single ring-shaped bundles. Ten specimens of ring-shaped bundles were tested using  
249 capstan grips with the same strain rate as before (Fig. 9). The gauge length was 220 mm  
250 (consistent to the ASTM D1414 Standard).

251 Finally, three specimens of 2nd-level hierarchical assembly were tested. The cross-  
252 sectional diameter of each specimen was measured as above (mean and SD between 30  
253 measurements in three different sections). The specimens were weighed with the same  
254 precision balance. In order to minimize the stress concentration, the specimens were  
255 tested directly on the stainless-steel 6-arms capstan grips, mounted on the Instron testing  
256 machine (Fig. 9).

257 The following indicators were considered: Yield Stress ( $\sigma_Y$ ), Yield Strain ( $\epsilon_Y$ ), Modulus  
258 of Elasticity ( $E$ ), Failure Force ( $F_F$ ), Failure Stress ( $\sigma_F$ ), Failure Strain ( $\epsilon_F$ ), Unit Work  
259 to Yield ( $L_Y$ ), Unit Work to Failure ( $L_F$ ) (Fig. 2). The force-displacement curves were  
260 converted to stress-strain curves using two different approaches:

- 261 • To describe the macroscopic mechanical behavior of the specimen, the apparent  
262 stress was computed dividing the force by the cross-sectional area measured  
263 before the test.
- 264 • To quantify the net mechanical properties, the net stress was also computed  
265 dividing the apparent stresses by the volume fraction ( $v$ ) of the specimens.
- 266 • The apparent and the net modulus of elasticity ( $E$ ), and unit works to failure  
267 were computed ( $L_Y$ ,  $L_F$ )

268 The volume fraction ( $v$ ) was calculated by using the equation:

$$269 \quad v = w/(L \cdot A \cdot \rho) \quad (\text{Eq. 1})$$

270 Where:

271  $w$  is the weight of the specimen

272  $L$  is length of the specimen,

273  $A$  is the cross-sectional area of the specimen

274  $\rho$  is the density of the raw material (Nylon 6,6 = 1.14 g/cm<sup>3</sup>)

### 275 **3. Results**

#### 276 *3.1. Comparison between random and aligned bundles*

277 The electrospun bundles of random and aligned Nylon 6,6 nanofibers were compared.

278 The random bundles had a cross-sectional diameter of  $0.52 \pm 0.05$  mm, and the aligned

279 bundles of  $0.52 \pm 0.06$  mm. The volume fraction ( $v$ ) for the random bundles was

280  $0.21 \pm 0.03$  and  $0.30 \pm 0.04$  for the aligned bundles.

#### 281 *3.1.2. Morphological investigation of the bundles*

282 The SEM investigation showed that the nanofibers of both the random bundles and the

283 aligned bundles were homogeneous, smooth, continuous, and with no defects such as

284 beads (Fig. 3). The nanofibers had consistent mean cross-sectional diameter of  $0.23 \pm$

285  $0.02$  micrometers. The different orientation of the nanofibers in the random and in the

286 aligned bundles was clearly visible.

287 The XCT investigation of the random bundles showed that nanofibers were randomly

288 arranged both on the surface and inside the bundle (Fig. 3). Few wrapping defects were

289 noted in the internal body of random bundles (Fig. 3).

#### 290 *3.1.3. Directionality of the nanofibers*

291 The Directionality analysis confirmed the different preferential orientation of the

292 nanofibers in the aligned bundles as opposed to the random ones (Fig. 4). The random

293 bundles showed a dispersion of the orientation of the nanofibers so that about 7% of

294 nanofibers fell in each bin. The aligned bundles had a predominant peak in the range of

295 0°-6° from the bundle axis ( $42.7\% \pm 3.1\%$  of the total), and a Gaussian-like distribution.  
296 A small amount of nanofibers of  $0.78\% \pm 0.15\%$  was perpendicular to the bundle (84°-  
297 90°).

#### 298 *3.1.4. Mechanical properties of the bundles*

299 The load-strain curves revealed a more deformable behavior for the random bundles and  
300 a stiffer behavior for the aligned bundles (Fig. 5). Both types of bundles showed a  
301 nonlinear toe region up to 1-4% strain (Fig. 5). The random bundles had a failure force  
302 of  $F_F = 3.27 \pm 0.61$  N, and were weaker than the aligned ones ( $F_F = 14.3 \pm 2.7$  N).

303 After the toe region, the random bundles showed a short elastic region up to an apparent  
304 yield stress of  $\sigma_Y = 3.27 \pm 0.90$  MPa and a final ductile region up to an apparent failure  
305 stress of  $\sigma_F = 15.6 \pm 2.8$  MPa (Fig. 5). The aligned bundles also showed higher apparent  
306 failure stress ( $\sigma_F = 68.7 \pm 15.0$  MPa) compared to the random bundles (Fig. 5). For both  
307 of the bundle types, the net mechanical properties were 3-5 times higher than the  
308 apparent ones (Table 1).

#### 309 *3.2 Properties of the hierarchical assemblies*

310 The ring-shaped bundles and the hierarchical assemblies made of such bundles were  
311 compared. The bundles used for the assemblies were homogeneous, and had a cross-  
312 sectional diameter of  $0.47 \pm 0.04$  mm. Three 2nd-level hierarchical assemblies were  
313 prepared, each with 24 ring-shaped bundles. The 2nd-level assemblies had a final cross-  
314 sectional diameter of  $4.3 \pm 0.57$  mm, and a length of 220 mm (Fig. 6). The bundles  
315 inside the assemblies were tightly grouped together and covered with a homogeneous  
316 nanofibrous sheath (Fig. 6). The volume fraction ( $\nu$ ) for the single bundles was  $\nu = 0.33$

317  $\pm 0.02$ . The 2nd-level hierarchical assemblies had a lower volume fraction  $\nu = 0.22 \pm$   
318  $0.05$ , due to the free-volume between the single bundles.

319 The 3rd-level hierarchical assembly had a cross-sectional diameter of  $4.6 \pm 0.17$  mm  
320 with a length of 220 mm. Observing the 3rd-level hierarchical assembly, the original  
321 2nd-level hierarchical assemblies were still distinguishable; they were tightly compacted  
322 inside the external nanofibrous sheath (Fig. 6). The volume fraction of the 3rd-level  
323 hierarchical assembly was  $\nu = 0.175$ .

### 324 *3.2.1 Morphology of the hierarchical assemblies*

325 The SEM investigation showed that the nanofibers in the hierarchical assemblies were  
326 homogeneous, smooth, continuous, and with no defects such as beads (Fig. 7). The  
327 nanofibers of the electrospun sheaths had consistent mean cross-sectional diameter of  
328  $0.23 \pm 0.03$  micrometers. The bundles were tightly grouped inside the nanofibrous  
329 sheaths (Fig. 7).

330 The XCT investigation on the 2nd-level hierarchical assemblies revealed that the sheath  
331 was homogeneous across the surface of the hierarchical assembly, with the presence of  
332 some circular defects. In the internal volume of the 2nd-level hierarchical assemblies,  
333 the bundles were axially aligned (Fig. 7). The XCT reconstructions of the 3rd-level  
334 hierarchical assembly showed that: (i) the nanofibrous sheaths were homogeneous, both  
335 the external and the internal with the presence of a few circular defects (Fig. 7) and (ii)  
336 the 2nd-level hierarchical assemblies forming the 3rd-level assembly were axially  
337 aligned, as well as the single bundles they were made of (Fig. 7).



338 *3.2.2 Alignment of nanofibers of the sheaths and of the internal bundles*

339 The Directionality investigation showed that the nanofibers of the sheaths for the  
340 hierarchical assemblies had a slight preferential circumferential orientation (Fig. 8):  
341 more than 45% of the nanofibers fell in the range of 66°-90° for the 2nd-level  
342 hierarchical assembly; more than 48% of the nanofibers fell in the range of 66°-90° for  
343 the 3rd-level assembly.

344 The preferential axial of alignment of the bundles and the nanofibers inside the bundles  
345 was confirmed by the XCT-based Directionality investigation (Fig. 8). All the  
346 specimens had a predominant peak in the range of 0°-6° and a Gaussian-like dispersion.  
347 The 2nd-level hierarchical assembly showed strong axial alignment, with 52.0% ± 5.1%  
348 in the range 0°-6°. Similarly, the 3rd-level hierarchical assembly had a strong axial  
349 alignment (47.3% ± 5.7% of the nanofibers were peak in the range of 0°-6° from the  
350 axis).

351 *3.2.3. Comparison of the mechanical properties of the single bundles and of the*  
352 *hierarchical assembly*

353 The typical load-strain curves of the single ring-shaped bundles and 2nd-level  
354 hierarchical assembly confirmed a brittle behavior with a nonlinear toe region up to 1 –  
355 4% of strain (Fig. 9). The single ring-shaped bundles showed a failure force of  $F_F =$   
356  $21.8 \pm 1.7$  N (mean and SD of ten specimens) and the 2nd-level hierarchical assemblies  
357 of  $F_F = 330 \pm 11.0$  N (mean and SD of three specimens) (Fig. 9).

358 The bundles had values of apparent failure stress  $\sigma_F = 63.4 \pm 10.9$  MPa ( $\epsilon_F = 9.29 \pm$   
359 1.02%) and the hierarchical assemblies of  $\sigma_F = 22.9 \pm 5.0$  MPa ( $\epsilon_F = 8.58 \pm 0.20\%$ )

360 respectively (Fig 9). The modulus of elasticity of the single bundles was  $E = 877 \pm 83.1$   
361 MPa and for the hierarchical assembly  $E = 343 \pm 87.0$  MPa (Fig. 9).  
362 The unit work to failure for the bundles was  $L_F = 0.25 \pm 0.08$  J/mm<sup>3</sup> and  $L_F = 0.08 \pm$   
363  $0.02$  J/mm<sup>3</sup> for the 2nd-level hierarchical assemblies (Fig. 9).  
364 The net mechanical properties (computed considering the volume fraction  $\nu$ ) were 4-6  
365 times higher than apparent ones (Table. 1).

#### 366 **4. Discussion**

367 The aim of the present study was to develop an innovative morphologically bioinspired  
368 electrospun nanofibrous assembly, by using non-resorbable Nylon 6,6, to replicate the  
369 hierarchical structure and the mechanical properties of a whole tendon or ligament.  
370 Nylon 6,6 was selected for its wide range of clinical applications, such as for suture  
371 wires and implantable non-resorbable devices [9].

372 In order to replicate every single hierarchical level of aggregation of the collagen fibrils  
373 inside the tendon and ligament tissue [3,4,14] (Fig. 6), different electrospun bundles  
374 were produced.

375 Firstly, random and aligned nanofiber bundles were obtained by means electrospinning  
376 Nylon 6,6 on a drum collector, rotating at different speed. In both cases, the nanofibers  
377 had the same diameter of the collagen fibrils [3,4,14] observed within tendons and  
378 ligaments. The random bundles were not satisfactory, because they had a morphology  
379 and an arrangement of the nanofibers, assessed with SEM and XCT imaging (Fig. 3),  
380 far from the tendon and ligament fascicles [36]. Furthermore, their mechanical  
381 properties were lower than the human tendon and ligament fascicle [14,37] (Fig. 5). For  
382 all these reasons the random bundles were discarded as candidates. The aligned bundles  
383 were selected as best fascicle-inspired candidates. Firstly, the SEM and the XCT images

384 (Fig. 3) confirmed that the morphology was similar to the collagen fascicles  
385 [3,14,36,38]. The Directionality analysis on the XCT scan of the aligned bundle (Fig.  
386 4) confirmed that the alignment of the Nylon 6,6 nanofibers was similar to that of the  
387 tendon and ligament collagen fibrils [39]. Finally, the apparent modulus of elasticity of  
388 our Nylon 6,6 aligned bundles ( $878 \pm 83$  MPa) was in the same range of the human  
389 tendon and ligament fascicles (between 63.5 and 317 MPa [14,37]). The apparent failure  
390 stress of the Nylon 6,6 aligned bundles ( $63.5 \pm 11.0$  MPa) was superior to the human  
391 tendon and ligament fascicles (between 6.8 and 28.1 MPa [14,37]) (Fig. 5). These  
392 findings are consistent with previous studies on electrospun bundles [25,27,40,41].  
393 Subsequently, in order to reproduce the whole structure of a tendon or ligament [3,4,14],  
394 several ring-shaped bundles were grouped together, obtaining the 2nd-level hierarchical  
395 assembly (Fig. 6). To do this, a dedicated procedure to electrospin sheath was developed  
396 (Fig. 1) in order to mimic the morphology of the epitenon/epiligament membranes of  
397 tendons and ligaments [3,4,14]. The Directionality analysis on XCT scans confirmed a  
398 pronounced axial alignment of the nanofibers inside the 2nd-level assembly, and a slight  
399 circumferential alignment of the nanofibers in the outer sheath. Compared to previous  
400 similar processes [42–46], our method allowed a finer tuning of the level of compaction  
401 of the bundles. In fact, the degree of circumferential orientation can be controlled  
402 through the electrospinning procedure by matching the process parameters (i.e.  
403 static/rotational time and the rotational speed of the device) during the production of the  
404 sheaths (Fig. 8). Thus, it was also possible to adjust the final cross-section of the  
405 assemblies themselves, improving their overall mechanical properties (Fig. 9).  
406 As this procedure was particularly flexible, we were able to produce 3rd-level  
407 hierarchical assemblies by grouping a number of 2nd-level hierarchical assemblies (Fig.  
408 6). The 3rd-level assemblies incorporate sheaths that mimicked the tendon and ligament

409 endotenon/endoligament membranes [3,4,14]. The Directionality analysis confirmed a  
410 pronounced axial alignment of the nanofibers inside the 3rd-level assembly. The slightly  
411 lower values of alignment for the 3rd-level assembly compared to the 2nd-level  
412 assemblies were caused by the higher percentage of nanofibers in the different sheaths  
413 forming the 3rd-level assembly. These hierarchical assemblies showed and  
414 unprecedented morphology, biomimicking every single collagen structure that compose  
415 a whole natural tendon or ligament [3,4,14].

416 Both the ring-shaped bundles and the 2nd-level hierarchical assemblies showed a  
417 nonlinear toe region up to 1-4% strain, similar to the behavior of the natural fascicles,  
418 tendons and ligaments (i.e. 1.5-4 %) [5,14,37]. After the toe region, both the bundles  
419 and the 2nd-level hierarchical assemblies exhibited a linear elastic behavior, up to 9%  
420 strain, before failing (again, similar to the behavior of the natural tendons and ligaments)  
421 (Fig. 9). The single bundles had a modulus of elasticity higher than the fascicles of  
422 tendons and ligaments [5,14,37]. The hierarchical assembly had a similar modulus of  
423 elasticity to natural tendons and ligaments (range: 20-3000 MPa [5,14]). The maximum  
424 strain of the bundles was in the same range of collagen fascicles and of natural tendons  
425 and ligaments (range: 9-25 % [5,37,47]). The failure strain of the hierarchical  
426 assemblies was in the range of the natural tendons and ligaments (range: 8-120 MPa  
427 [5,14]). The apparent failure stress of the bundles was  $\sigma_F = 63.4 \pm 10.9$  MPa. These  
428 values were higher than the fascicles of natural tendons and ligaments (range: 6-40 MPa  
429 [5,37,47]). The apparent failure stress for the hierarchical assemblies was  $\sigma_F = 22.9 \pm$   
430 5.0 MPa, which is in the same range observed in natural tendons and ligaments (range:  
431 1-116 MPa [5,14]). As expected, the modulus of elasticity and the failure stress of the  
432 2nd-level hierarchical assembly was lower than that of the single bundles. This may be  
433 due to the fact that the apparent stress in the hierarchical assembly is calculated over the

434 total cross-sectional area (which includes the actual cross-section of the bundles, but  
435 also some unavoidable empty space). Similarly, the values of net stress (i.e. computed  
436 considering the volume fraction actually filled by nanofibers) were significantly higher  
437 (4-6 times) than the apparent ones.

438 Altogether, these properties can grant excellent mechanical performance, and a  
439 biomimetic behavior of the hierarchical assembly. Considering that the Nylon 6,6 is an  
440 inert material, the possible applications in reconstructive surgery could include  
441 replacement of injured tendons or ligaments for the elderly patients (i.e. age greater than  
442 60 years). In fact, due to the low metabolic activity in the elderly, regenerative medicine  
443 (i.e. resorbable scaffolds) is not recommended.

444 Most of the previous electrospun scaffolds reported for tendon and ligament  
445 replacements consist of braided, twisted or knitted fibers [46,48–52] which do not  
446 replicate the morphology of natural tissues. Compared to previous literature results, the  
447 method herein proposed to produce electrospun sheaths confers a better compaction of  
448 the single bundles in the multiscale hierarchical scaffold [46,48–52]; thus, providing  
449 optimal compromise between morphology and mechanical properties.

450 Moreover, such high biofidelic hierarchical assemblies will also be suitable as artificial  
451 tendons or ligaments for *in vitro* biomechanical validations tests or surgical training. In  
452 fact, to the best of our knowledge, there are no specific devices available on the market  
453 for such applications. The previous attempts in this field were absolutely trivial and not  
454 biomimetic [53–55].

455 A limitation of this study should be mentioned: some droplets were created during  
456 deposition of the electrospun sheaths (Fig. 7). Such defects might have reduced the  
457 ability of the sheath to tightly bind the bundles together which might have reduced the  
458 improvement in mechanical properties deriving from the compaction of the bundles. In

459 the future, these defects could be avoided by optimizing the flow rate of the Nylon 6,6  
460 solution, possibly further improving the mechanical strength of the assemblies.

461 The XCT investigation was extremely challenging because of the small diameter of the  
462 electrospun nanofibers, and of the low attenuation of the polymer [31,41,51,52,56,57].

463 Videos of the XCT scans of a single bundle of aligned nanofibers and of 2nd-level  
464 hierarchical assembly are available in the Supplementary Materials through  
465 ScienceDirect. Additional images and videos of the XCT scans are available through  
466 Figshare (single aligned bundle: <https://doi.org/10.6084/m9.figshare.7636580.v4>; 2nd-  
467 level hierarchical assembly: <https://doi.org/10.6084/m9.figshare.7636592.v3>; 3rd-level  
468 hierarchical assembly: <https://doi.org/10.6084/m9.figshare.7636595.v3> ).

469 In conclusion this work showed an innovative electrospinning production process to  
470 design and build nanofibrous Nylon 6,6 hierarchical assemblies, suitable as future  
471 implantable devices, able to mimic the multiscale morphology and the biomechanical  
472 properties of tendons and ligaments.

473

474 **Acknowledgments**

475 The Italian Ministry of University and Research (MIUR) is acknowledged. The mobility  
476 of Alberto Sensini was funded by the University of Bologna (Marco Polo grant). The  
477 Zeiss Global Centre at the University of Portsmouth is greatly acknowledged for the  
478 support in X-ray imaging and data post-processing. The authors gratefully acknowledge  
479 the Giuseppe Valli for the valuable suggestions and for 3D-printing the 6-arms capstan  
480 grips.

481

482 **Competing interest:** None declared.

483

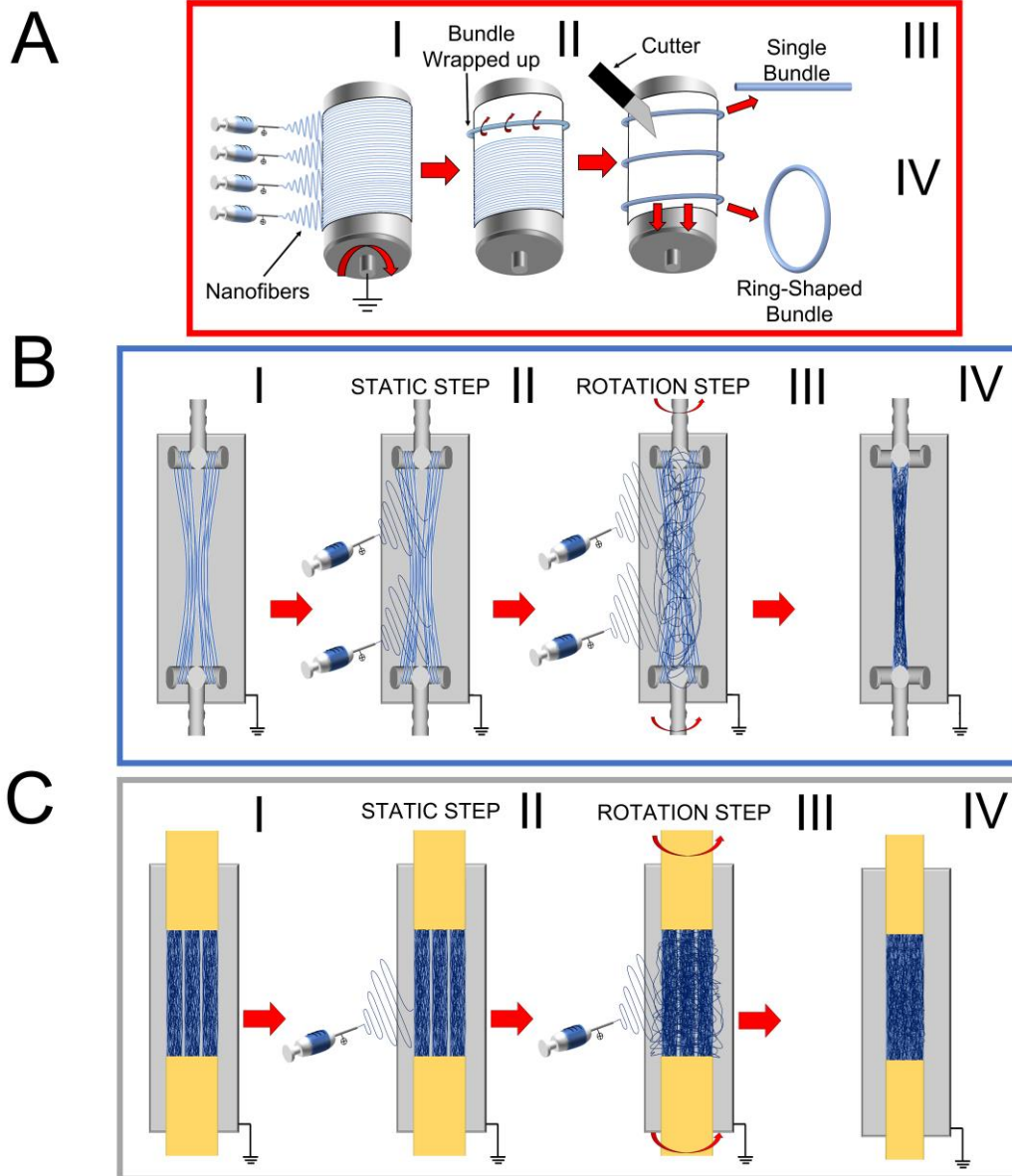
484 **Funding:** Funding from the Italian Ministry of University and Research (MIUR) is  
485 acknowledged. The mobility of Alberto Sensini was funded by the University of  
486 Bologna (Marco Polo grant).

487

488 **Ethical approval:** Not required.

489

490 **Figure Captions**

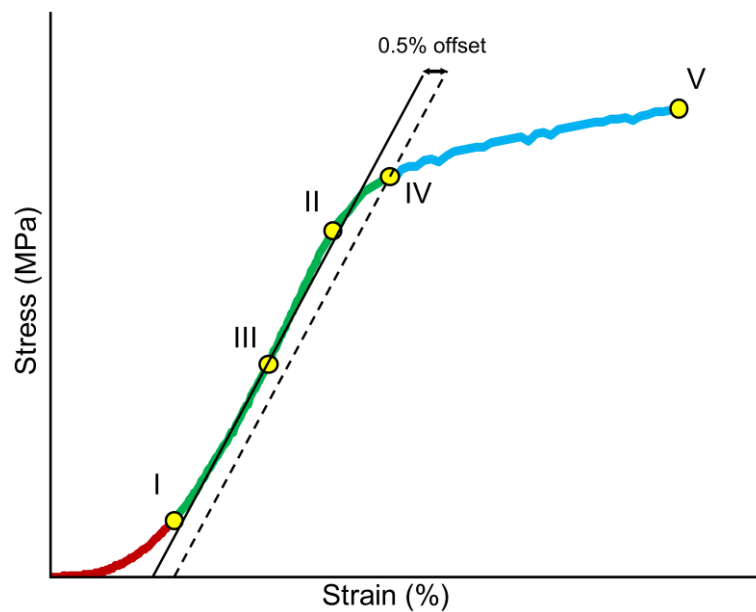


491

492 **Fig. 1** - Electrospinning setups and procedures to produce the bundles and the  
 493 hierarchical devices. A) Bundles production: I) random or aligned nanofibers were  
 494 electrospun on the rotating drum collector; II) mats of nanofibers cut in strips and  
 495 manually wrapped to obtain the bundles; III) Some bundles were cut for remove them  
 496 from the drum (single bundles); IV) other bundles were removed from the drum without  
 497 cutting (ring-shaped bundles). B) 2nd-level hierarchical assembly production: I) ring-  
 498 shaped bundles of aligned nanofiber were hooked on the 6-arms capstan grip; II)  
 499 electrospun sheath production during the static step; III) during the rotation step the mat



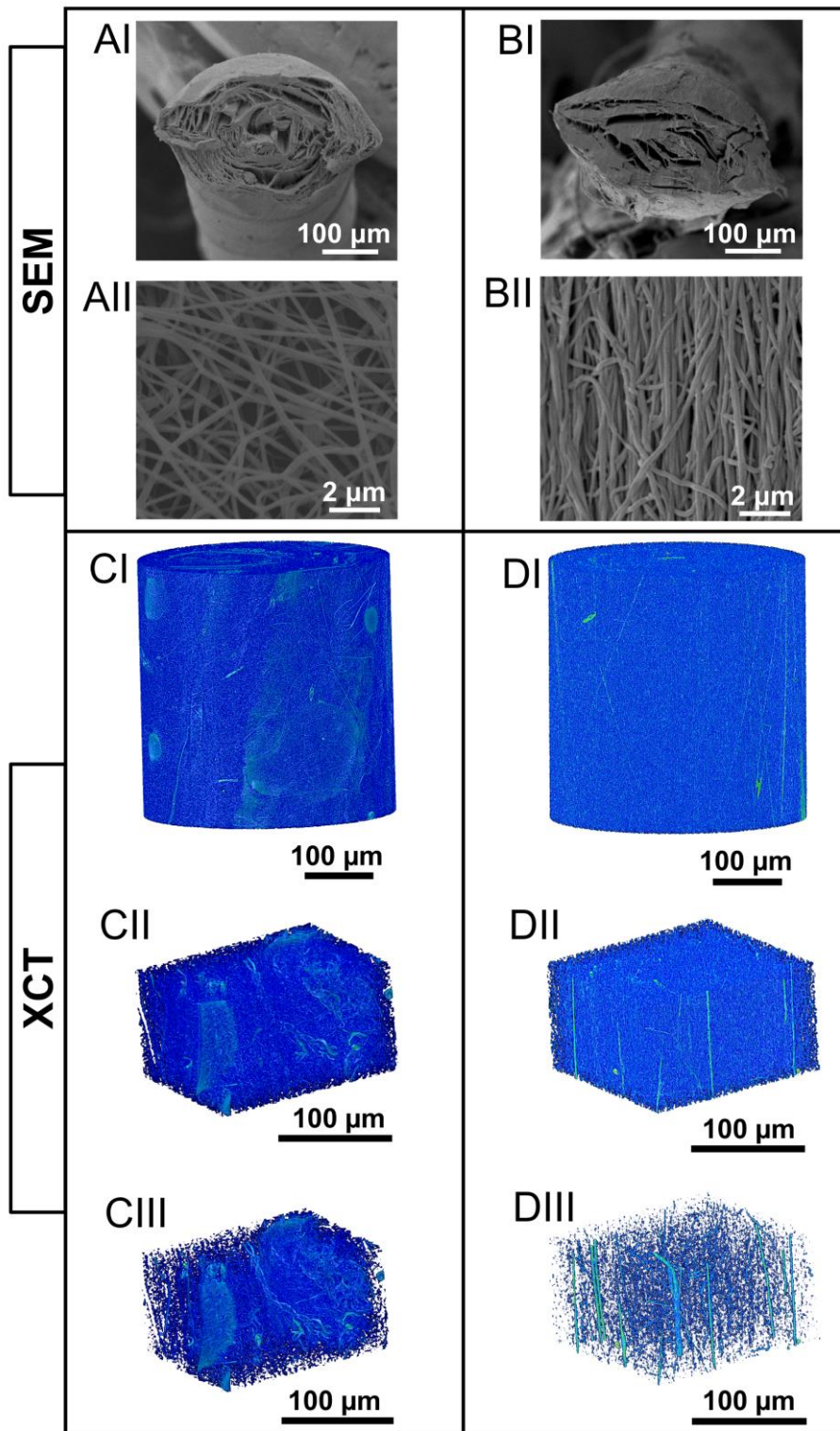
500 of nanofibers was torn from one side of the collector and wrapped around the group of  
501 bundles; IV) final 2nd-level hierarchical assembly ready to be tested. B) 3rd-level  
502 hierarchical assembly production: I) three 2nd-level hierarchical assembly grouped  
503 together; II) electrospun sheath production during the static step; III) during the rotation  
504 step the mat of nanofibers was torn from one side of the collector and wrapped around  
505 the group of 2nd-level hierarchical assembly; IV) final 3rd-level hierarchical assembly  
506 ready to be characterized.



507

508 **Fig. 2** - Post processing of the stress-strain curves. The stress-strain curves were  
509 qualitatively similar for the single bundles and for the hierarchical assemblies, but the  
510 magnitude of the stress and strain achieved were different. The failure stress ( $\sigma_F$ ) (V)  
511 was identified as the highest stress in the entire curve. The starting point of the linear  
512 region (I) was identified as 20% of the failure stress ( $\sigma_F$ ) for the bundles of aligned  
513 nanofibers and the 2nd-level hierarchical assembly, and as 5% of the failure stress ( $\sigma_F$ )  
514 for the bundles of random nanofibers (the different threshold was required due to the  
515 different behaviour of the two types of bundle). The initial toe region (from 0 N to I)

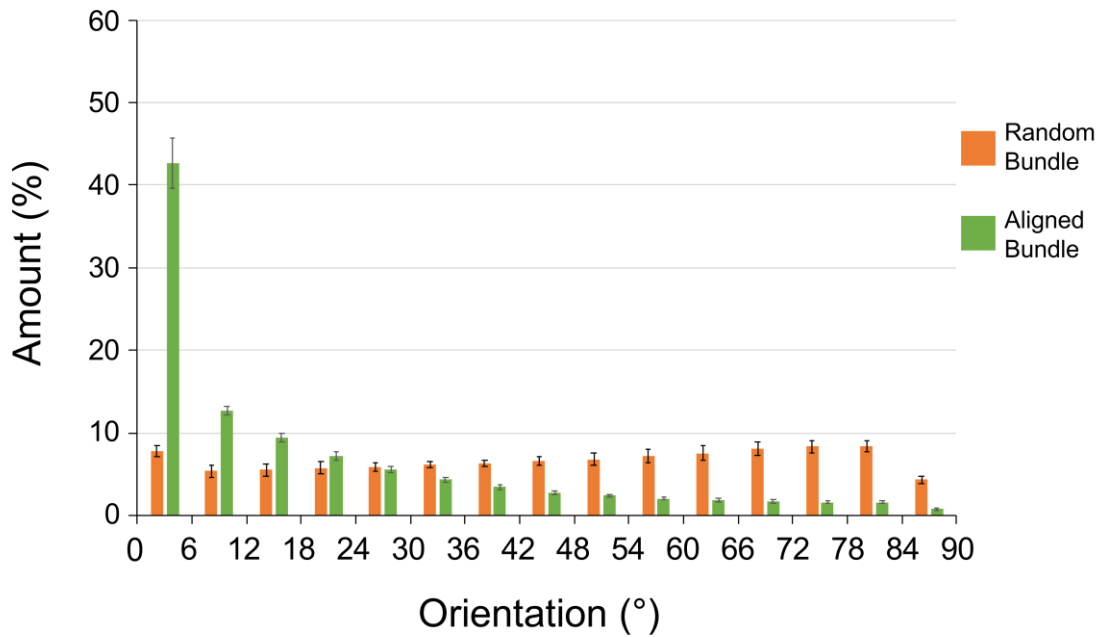
516 was disregarded. An initial guess for the yield strain was visually identified (II). A first  
517 linear regression (solid line) was applied to the first 50% of the linear region, between  
518 points (I) and (III) (III was half-way between I and II). A second line parallel to the first  
519 regression was drawn with an offset of 0.5% strain (dashed line). The limit of  
520 proportionality was defined with the 0.5%-strain offset criterion as the intersection (IV)  
521 between the latter line and the stress-strain curve. The modulus of elasticity (E) was  
522 calculated as the slope of a new regression line between (I) and (IV). The unit work to  
523 yield ( $L_Y$ ) and to failure ( $L_F$ ) were calculated as the integrals under the curves (with the  
524 method of trapezoids). Two plots were obtained for each specimen: one reporting the  
525 apparent stress, the other one with the net stress.



526

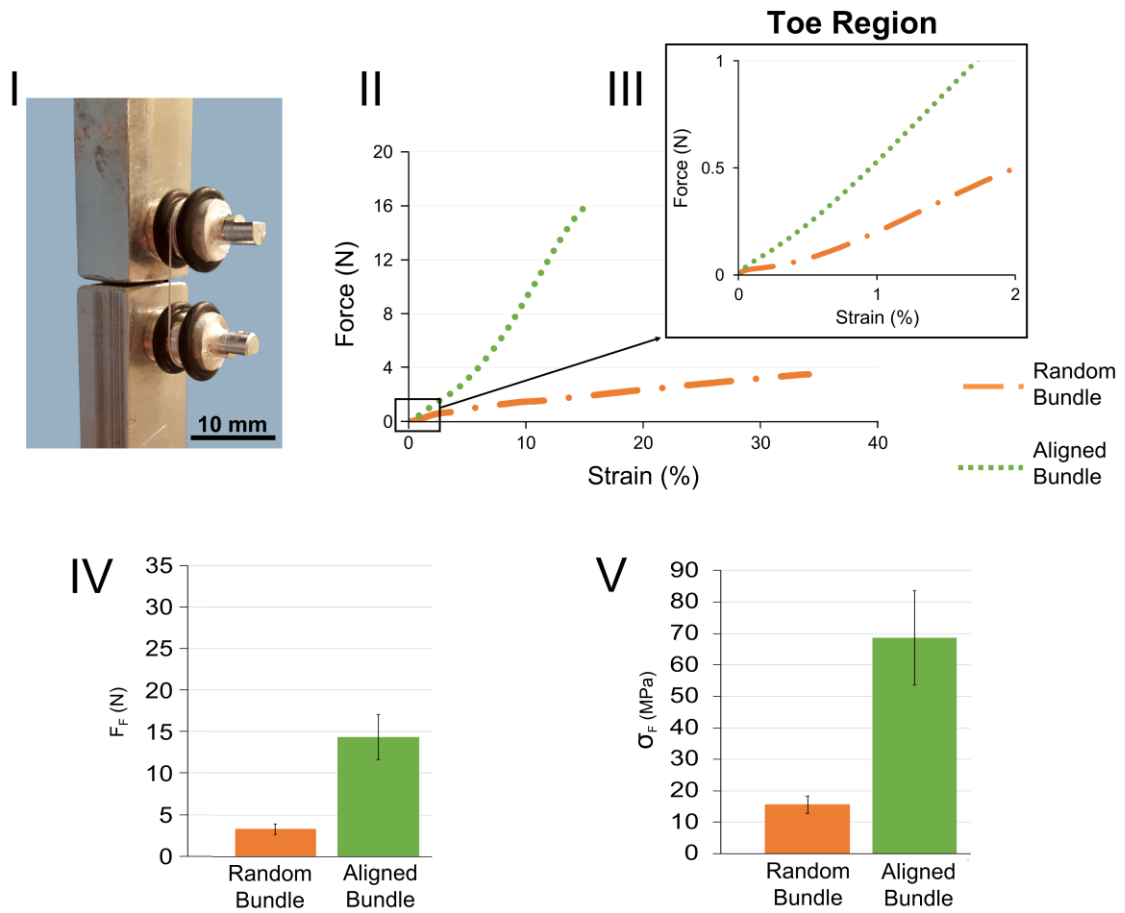
527 **Fig. 3** - Imaging of the random and of the aligned bundles. A) SEM images of a random  
 528 nanofiber bundle. B) SEM images of an aligned nanofiber bundle. The sections of the  
 529 bundles (magnification = 100x) are visible in part I; the surface of the bundle  
 530 (magnification = 8000x) are visible in part II. C) XCT images of a random nanofiber

531 bundle; D) XCT images of an aligned nanofiber bundle (0.4 micrometers of voxel size).  
532 The sections of the bundles are visible in part I; an internal crop showing the alignment  
533 of the nanofibers inside the bundle is reported in part II; tuning the thresholding the most  
534 internal nanofibers become visible in part III.



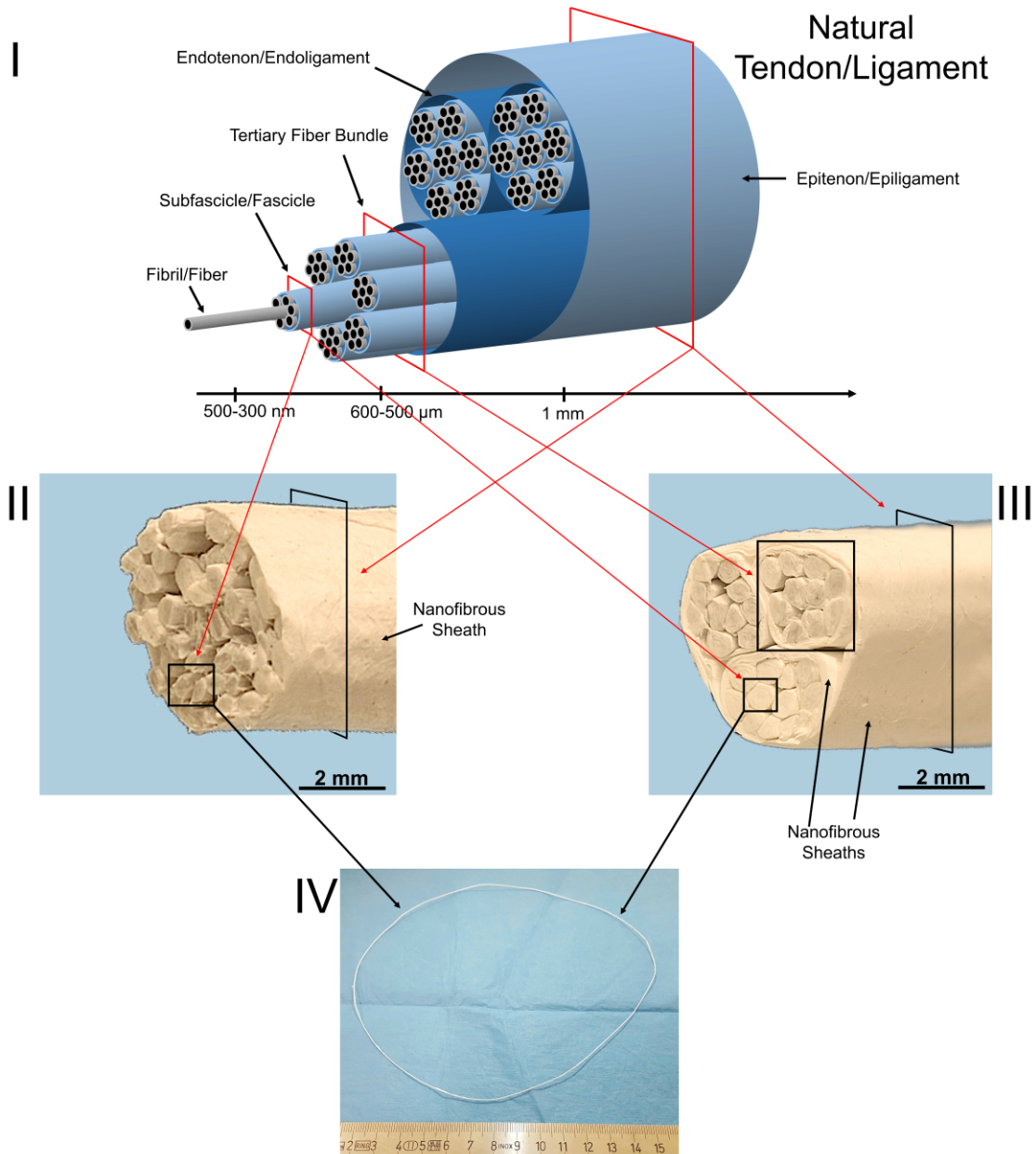
535

536 **Fig. 4** - Directionality of the nanofibers in the random and in the aligned bundles. The  
537 directionality histograms show the distribution of the nanofibers in the different  
538 directions for the two types of bundles. An angle of 0° means that the nanofibers were  
539 aligned with the axis of the bundle, an angle of 90° means that the nanofibers were  
540 perpendicular to the bundle.



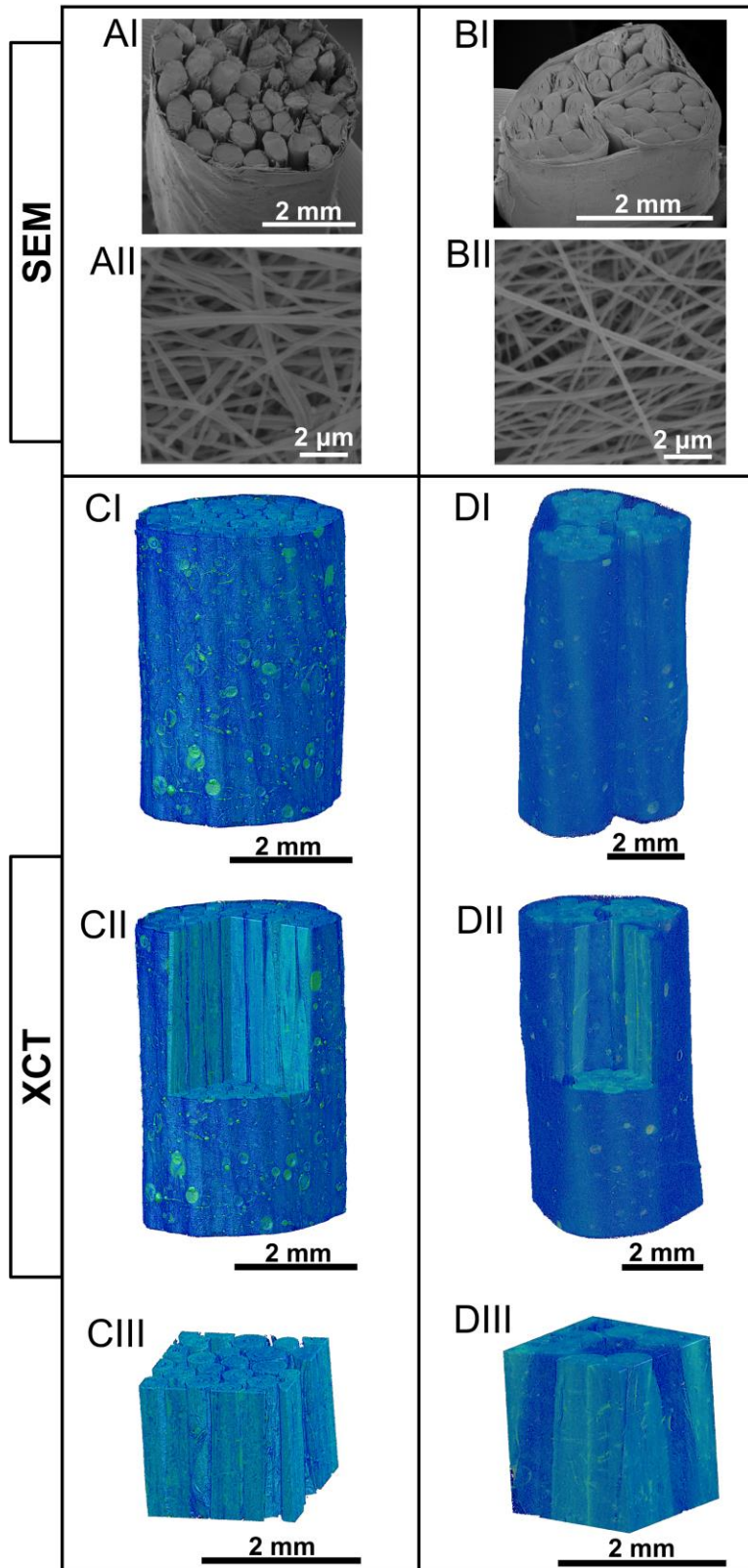
541

542 **Fig. 5** - Mechanical characterization of the bundles of random nanofiber bundles and of  
 543 aligned nanofibers. I) Tensile test setup with custom-made capstan grips. II) typical  
 544 load-strain curves of the random bundles and the aligned bundles; III) zoom-in of the  
 545 nonlinear toe region. Comparison between the mechanical properties of the random and  
 546 of the aligned bundles: IV) failure force ( $F_F$ ); V) apparent failure stress ( $\sigma_F$ ). The  
 547 corresponding net mechanical properties are reported in Table 1.



548

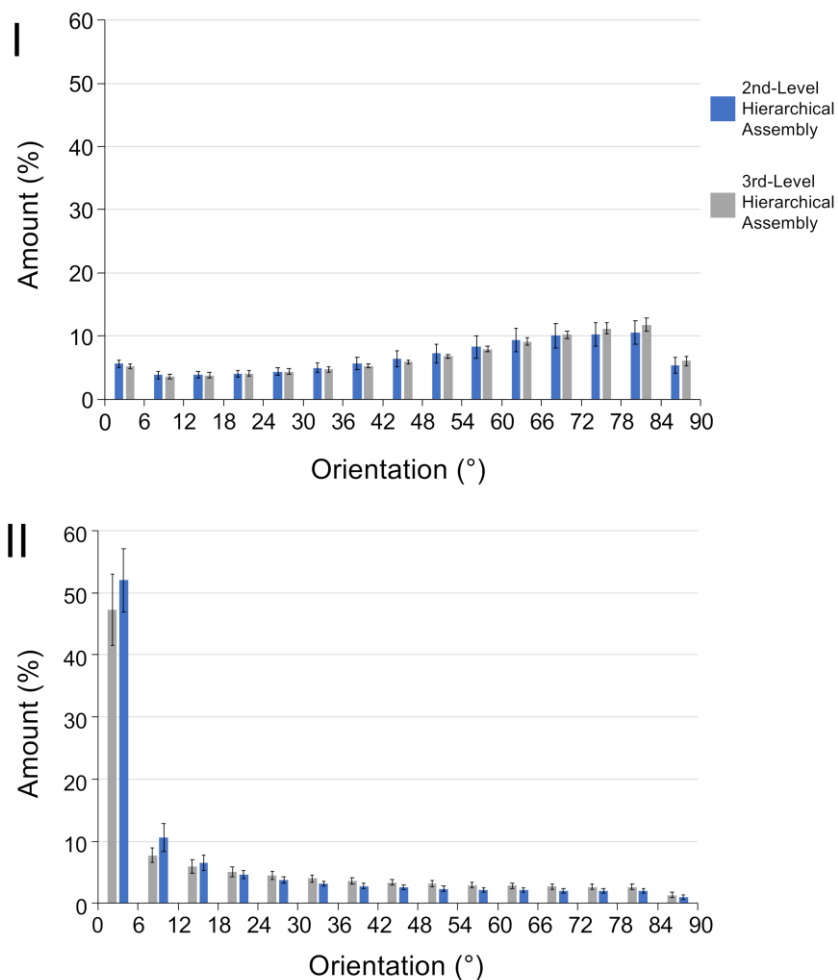
549 **Fig. 6** - Comparison between a natural tendon or ligament and the electrospun  
 550 hierarchical assemblies. I) Hierarchical structure of a tendon or ligament [4]. II) Image  
 551 of the cross-section of a 2nd-level hierarchical assembly. III) Image of the cross-section  
 552 of a 3rd-level hierarchical assembly. IV) Image of a ring-shaped bundle used to build  
 553 the hierarchical assemblies.



554

555 **Fig. 7** - Imaging of the of the 2nd-level and 3rd-level hierarchical assemblies. A) SEM  
 556 images of a 2nd-level hierarchical assembly. B) SEM images of a 3rd-level hierarchical

557 assembly. The sections of the hierarchical assemblies (magnification = 25x) are visible  
 558 in part I; the nanofibers on the surface of the electrospun sheaths (magnification =  
 559 8000x) are visible in part II. C) XCT images of a 2nd-level hierarchical assembly (5.27  
 560 micrometers voxel size). D) XCT images of a 3rd-level hierarchical assembly (5.27  
 561 micrometers voxel size). An external section showing the external electrospun sheath  
 562 is visible in part I; an external crop showing the internal axially aligned bundles is  
 563 reported in part II; an internal crop showing the most internal axially aligned bundles  
 564 are visible in part III.

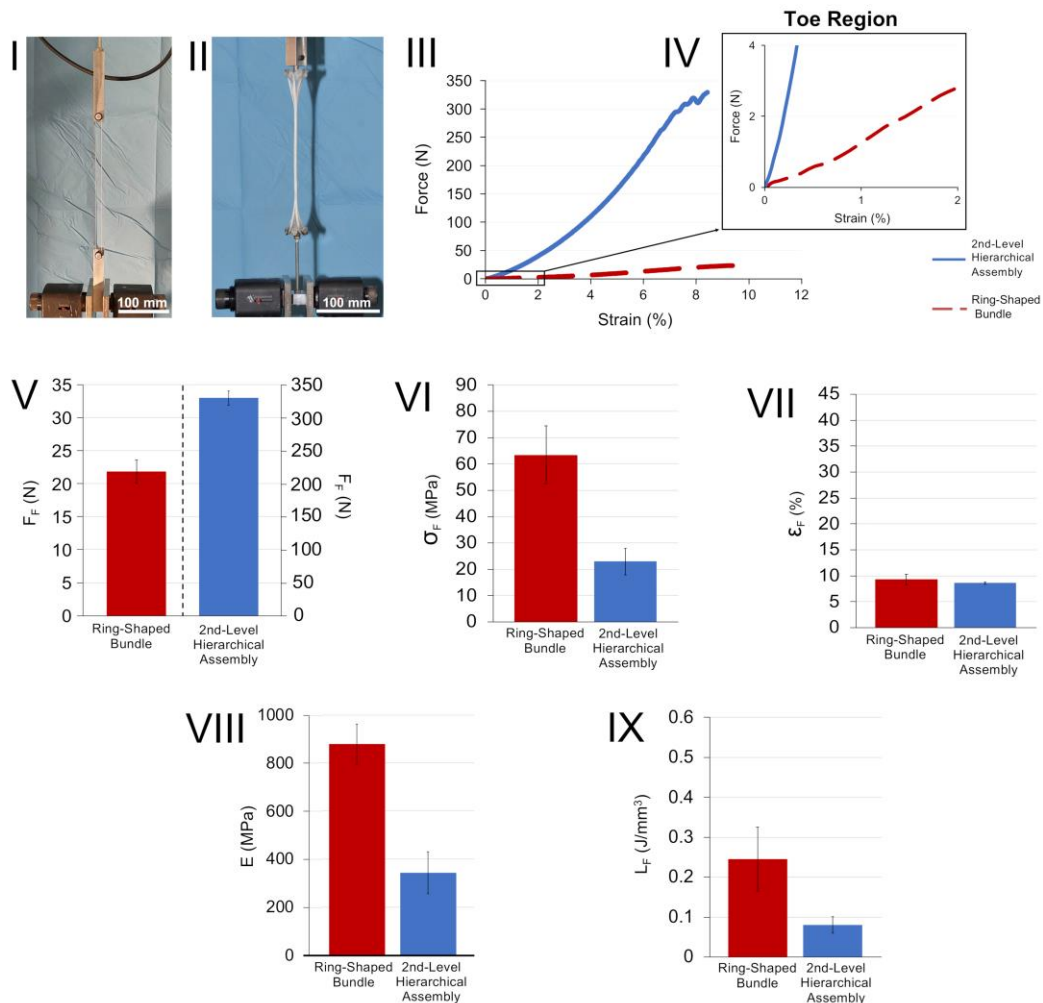


565

566 **Fig. 8** - Comparison between the alignment of the nanofibers in the outer sheaths (I) and  
 567 inside the assemblies (II) for the 2nd-level and the 3rd-level hierarchical assemblies. An



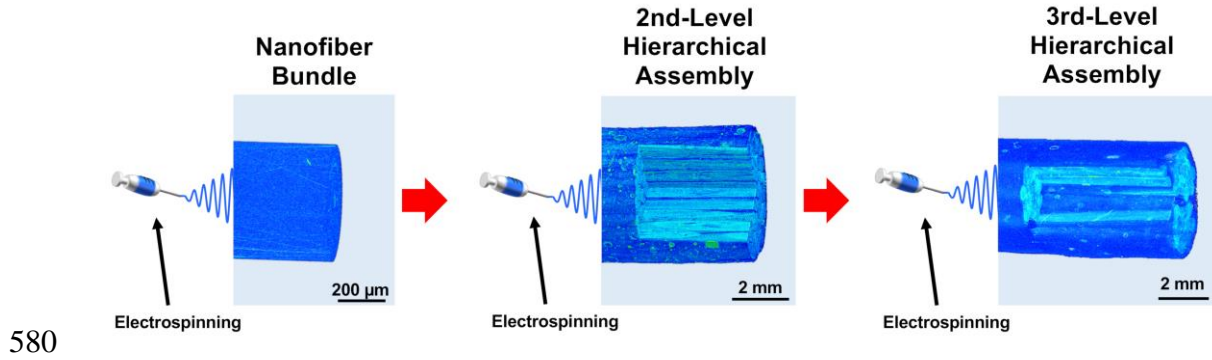
568 angle of  $0^\circ$  means that the nanofibers were aligned with the axis of the bundle,  $90^\circ$  means  
 569 that the nanofibers were perpendicular to the bundle.



570

571 **Fig. 9** - Mechanical characterization of the ring-shaped bundles and of the 2nd-level  
 572 hierarchical assembly. I) tensile testing of the ring-shaped bundles using custom-made  
 573 capstan grips; II) tensile testing of the 2nd-level hierarchical assembly using the 6-arms  
 574 capstan grips. III) typical load-strain curves of the ring aligned nanofiber bundles and  
 575 of the 2nd-level hierarchical assemblies; IV) zoom-in the nonlinear toe regions.  
 576 Comparison between the mechanical properties of the bundles and the 2nd-level  
 577 hierarchical assemblies: V) failure force ( $F_F$ ); VI) apparent failure stress ( $\sigma_F$ ); VII)

578 failure strain ( $\epsilon_F$ ); VIII) apparent modulus of elasticity (E); IX) apparent unit work to  
579 failure ( $L_F$ ). The corresponding net mechanical properties are reported in Table 1.



581 **Graphical Abstract**

582

## Tables

**Table 1.** Net mechanical properties of the bundles and the 2nd-level hierarchical assemblies obtained from the apparent ones, considering the fraction of volume ( $v$ ) actually taken by the nanofibers.

	Yield stress (MPa)	Failure stress (MPa)	Modulus of Elasticity (MPa)	Unit work to failure (J/mm <sup>3</sup> )
Random Bundle	15.6 ± 3.12	75.5 ± 13.1	-	-
Aligned Bundle	-	235 ± 28.6	-	-
Ring-shaped Bundle	-	389 ± 65.3*	5390 ± 421.1	1.56 ± 0.484
2nd-level Hierarchical Assembly	-	106 ± 4.04*	1589 ± 41.20	0.372 ± 0.0200

Note\*: a slightly lower failure stress was found for the aligned bundles compared to the ring-shaped ones, in relation to the different gripping system (the gripping system used in the first case induced a higher stress concentration than with the ring-shaped bundles)

## References

- [1] Abbah SA, Spanoudes K, O'Brien T, Pandit A, Zeugolis D. Assessment of stem cell carriers for tendon tissue engineering in pre-clinical models. *Stem Cell Res Ther* 2014;5:1–9. doi:10.1186/scrt426.
- [2] Zeugolis DI, Chan JCY, Pandit A. Tendons: Engineering of Functional Tissues. In: Pallua N, Suscheck C, editors. *Tissue Eng. From Lab to Clin. Tissue Eng.* Springer Berlin Heidelberg; 2011, p. 1–634. doi:10.1007/978-3-642-02824-3.
- [3] Kastelic J, Galeski A, Baer E. The Multicomposite Structure of Tendon. *Connect Tissue Res* 1978;6:11–23. doi:10.3109/03008207809152283.
- [4] Kannus P. Structure of the tendon connective tissue. *Scand J Med Sci Sport* 2000;10:312–20. doi:10.1034/j.1600-0838.2000.010006312.x.
- [5] Goh KL, Listrat A, Béchet D. Hierarchical mechanics of connective tissues: Integrating insights from nano to macroscopic studies. *J Biomed Nanotechnol* 2014;10:2464–507. doi:10.1166/jbn.2014.1960.
- [6] McCarthy MM, Hannafin JA. The Mature Athlete: Aging Tendon and Ligament. *Sports Health* 2014;6:41–8. doi:10.1177/1941738113485691.
- [7] Woo SLY, Hollis JM, Adams DJ, Lyon RM, Takai S. Tensile properties of the human femur-anterior cruciate ligament-tibia complex: The effects of specimen age and orientation. *Am J Sports Med* 1991;19:217–25. doi:10.1177/036354659101900303.
- [8] Chen J, Xu J, Wang A, Zheng M. Scaffolds for tendon and ligament repair: review of the efficacy of commercial products. *Expert Rev Med Devices* 2014;6:61–73. doi:10.1586/17434440.6.1.61.
- [9] Maitz MF. Applications of synthetic polymers in clinical medicine. *Biosurface and Biotribology* 2015;1:161–76. doi:10.1016/j.bsbt.2015.08.002.
- [10] Capperauld I. Suture materials: A review. *Clin Mater* 1989;4:3–12. doi:10.1016/0267-6605(89)90021-8.
- [11] Boileau P, Brassart N, Watkinson DJ, Carles M, Hatzidakis AM, Krishnan SG. Arthroscopic repair of full-thickness tears of the supraspinatus: Does the tendon really heal? *J Bone Jt Surg - Ser A* 2005;87:1229–40. doi:10.2106/JBJS.D.02035.
- [12] Longo UG, Lamberti A, Maffulli N, Denaro V. Tendon augmentation grafts: A systematic review. *Br Med Bull* 2010;94:165–88. doi:10.1093/bmb/ldp051.
- [13] Jackson DW, Heinrich JT, Simon TM. Biologic and synthetic implants to replace the anterior cruciate ligament. *Arthrosc J Arthrosc Relat Surg* 1994;10:442–52. doi:10.1016/S0749-8063(05)80197-5.
- [14] Murphy W, Black J, Hastings G. *Handbook of Biomaterial Properties*. Second. Springer; 2016. doi:10.1007/978-1-4939-3305-1.
- [15] Batty LM, Norsworthy CJ, Lash NJ, Wasiak J, Richmond AK, Feller JA. Synthetic devices for reconstructive surgery of the cruciate ligaments: A

- systematic review. *Arthrosc - J Arthrosc Relat Surg* 2015;31:957–68. doi:10.1016/j.arthro.2014.11.032.
- [16] Brunet P, Charrois O, Degeorges R, Boisrenoult P, Beaufils P. Reconstruction of acute posterior cruciate ligament tears using a synthetic ligament. *Rev Chir Orthop Reparatrice Appar Mot* 2005;91:34–43. doi:MDOI-RCO-02-2005-91-1-0035-1040-101019-200510479 [pii].
- [17] Engstrom B, Wredmark T, Westblad P. Patellar tendon or Leeds-Keio graft in the surgical treatment of anterior cruciate ligament ruptures. Intermediate results. *Clin Orthop Relat Res* 1993:190–7.
- [18] Ochi M, Yamanaka T, Sumen Y, Ikuta Y. Arthroscopic and histologic evaluation of anterior cruciate ligaments reconstructed with the Leeds-Keio ligament. *Arthrosc J Arthrosc Relat Surg* 1993;9:387–93. doi:10.1016/S0749-8063(05)80312-3.
- [19] Rading J, Peterson L. Clinical Experience with the Leeds-Keio Artificial Ligament in Anterior Cruciate Ligament Reconstruction: A Prospective Two-Year Follow-up Study. *Am J Sports Med* 1995;23:316–9. doi:10.1177/036354659502300311.
- [20] Murray AW, Macnicol MF. 10–16 year results of Leeds-Keio anterior cruciate ligament reconstruction. *Knee* 2004;11:9–14. doi:doi:10.1016/S0968-0160Ž03.00076-0.
- [21] Hirooka A, Yoneda M, Wakaitani S, Isaka Y, Hayashida K, Fukushima S, et al. Augmentation with a Gore-Tex patch for repair of large rotator cuff tears that cannot be sutured. *J Orthop Sci* 2002;7:451–6. doi:10.1007/s007760200078.
- [22] Kollender Y, Bender B, Weinbroum AA, Nirkin A, Meller I, Bickels J. Secondary reconstruction of the extensor mechanism using part of the quadriceps tendon, patellar retinaculum, and gore-tex strips after proximal tibial resection. *J Arthroplasty* 2004;19:354–60. doi:10.1016/j.arth.2003.11.004.
- [23] Muren O, Dahlstedt L, Brosjö E, Dahlborn M, Dalén N. Gross osteolytic tibia tunnel widening with the use of Gore-Tex anterior cruciate ligament prosthesis: A radiological, arthrometric and clinical evaluation of 17 patients 13-15 years after surgery. *Acta Orthop* 2005;76:270–4. doi:10.1080/00016470510030689.
- [24] Miller MD, Peters CL, Allen B. Early Aseptic Loosening of a Total Knee Arthroplasty Due to Gore-Tex Particle-Induced Osteolysis. *J Arthroplasty* 2006;21:765–70. doi:10.1016/j.arth.2005.07.021.
- [25] O'Connor RA, McGuinness GB. Electrospun nanofibre bundles and yarns for tissue engineering applications: A review. *Proc Inst Mech Eng Part H J Eng Med* 2016;230:987–98. doi:10.1177/0954411916656664.
- [26] Brennan DA, Conte AA, Kanski G, Turkula S, Hu X, Kleiner MT, et al. Mechanical Considerations for Electrospun Nanofibers in Tendon and Ligament Repair. *Adv Healthc Mater* 2018;1701277:1–31. doi:10.1002/adhm.201701277.
- [27] Sensini A, Cristofolini L. Biofabrication of Electrospun Scaffolds for the Regeneration of Tendons and Ligaments. *Materials (Basel)* 2018;11:1963.

doi:10.3390/ma11101963.

- [28] Liu Z. Scale space approach to directional analysis of images. *Appl Opt* 1991;30:1369–73. doi:<https://doi.org/10.1364/AO.30.001369>.
- [29] Schindelin J, Arganda-Carreras I, Frise E, Kaynig V, Longair M, Pietzsch T, et al. Fiji: an open-source platform for biological-image analysis. *Nat Methods* 2012;9:676–82. doi:10.1038/nmeth.2019.
- [30] Schneider CA, Rasband WS, Eliceiri KW. NIH Image to ImageJ: 25 years of image analysis. *Nat Methods* 2012;9:671–5. doi:10.1038/nmeth.2089.
- [31] Sensini A, Cristofolini L, Focarete ML, Belcari J, Zucchelli A, Kao A, et al. High-resolution x-ray tomographic morphological characterisation of electrospun nanofibrous bundles for tendon and ligament regeneration and replacement. *J Microsc* 2018;272:196–206. doi:10.1111/jmi.12720.
- [32] Butler DL. Anterior cruciate ligament: its normal response and replacement. *J Orthop Res* 1989;7:910–21. doi:10.1002/jor.1100070618.
- [33] Lewis G, Shaw KM. Tensile properties of human tendo Achillis: effect of donor age and strain rate. *J Foot Ankle Surg* 1997;36:435–45. doi:10.1016/S1067-2516(97)80096-8.
- [34] Wren TA., Yerby SA, Beaupré GS, Carter DR. Mechanical properties of the human achilles tendon. *Clin Biomech* 2001;16:245–51. doi:10.1016/S0268-0033(00)00089-9.
- [35] Lee M, Hyman W. Modeling of failure mode in knee ligaments depending on the strain rate. *BMC Musculoskelet Disord* 2002;3:1–8. doi:<https://doi.org/10.1186/1471-2474-3-3>.
- [36] Moshiri A, Oryan A. Tendon and Ligament Tissue Engineering, Healing and Regenerative Medicine. *J Sports Med Doping Stud* 2013;3:1–18. doi:10.4172/2161-0673.1000126.
- [37] Hanson P, Aagaard P, Magnusson SP. Biomechanical properties of isolated fascicles of the Iliopsoas and Achilles tendons in African American and Caucasian men. *Ann Anat* 2012;194:457–60. doi:10.1016/j.aanat.2012.03.007.
- [38] Kannus P, Paavola M, Józsa L. Aging and degeneration of tendons. In: Maffulli N, Renström P, W.B. L, editors. *Tendon Inj.*, London: Springer; 2005, p. 25–31. doi:10.1007/1-84628-050-8\_4.
- [39] Provenzano PP, Vanderby R. Collagen fibril morphology and organization: Implications for force transmission in ligament and tendon. *Matrix Biol* 2006;25:71–84. doi:10.1016/j.matbio.2005.09.005.
- [40] Sensini A, Gualandi C, Cristofolini L, Tozzi G, Dicarolo M, Teti G, et al. Biofabrication of bundles of poly(lactic acid)-collagen blends mimicking the fascicles of the human Achille tendon. *Biofabrication* 2017;9. doi:10.1088/1758-5090/aa6204.
- [41] Sensini A, Gualandi C, Zucchelli A, Boyle L, Kao AP, Reilly GC, et al. Tendon Fascicle-Inspired Nanofibrous Scaffold of Polylactic acid/Collagen with

- Enhanced 3D-Structure and Biomechanical Properties. *Sci Rep* 2018;8:1–15. doi:<https://doi.org/10.1038/s41598-018-35536-8>.
- [42] Zhou FL, Gong R-H, Porat I. Nano-coated hybrid yarns using electrospinning. *Surf Coatings Technol* 2010;204:3459–63. doi:10.1016/j.surfcoat.2010.04.021.
- [43] Kohlman LW, Roberts GD. Method for coating tow with an electrospun nanofiber. US8932683B1, 2015. doi:10.1016/j.(73).
- [44] Naghashzargar E, Farè S, Catto V, Bertoldi S, Semnani D, Karbasi S, et al. Nano/micro hybrid scaffold of PCL or P3HB nanofibers combined with silk fibroin for tendon and ligament tissue engineering. *J Appl Biomater Funct Mater* 2015;13:e156–68. doi:10.5301/jabfm.5000216.
- [45] Li D, Pan X, Sun B, Wu T, Chen W, Huang C, et al. Nerve conduits constructed by electrospun P(LLA-CL) nanofibers and PLLA nanofiber yarns. *J Mater Chem B* 2015;3:8823–31. doi:10.1039/C5TB01402F.
- [46] Banik BL, Lewis GS, Brown JL. Multiscale Poly-( $\epsilon$ -caprolactone) Scaffold Mimicking Non-linearity in Tendon Tissue Mechanics. *Regen Eng Transl Med* 2016;2:1–9. doi:10.1007/s40883-016-0008-5.
- [47] Butler DL, Kay MD, Stouffer DC. Fascicle-Bone Units From Human Patellar Tendon and Knee Ligaments. *J Biomech* 1986;19:425–32. doi:[https://doi.org/10.1016/0021-9290\(86\)90019-9](https://doi.org/10.1016/0021-9290(86)90019-9).
- [48] Xu Y, Dong S, Zhou Q, Mo X, Song L, Hou T, et al. The effect of mechanical stimulation on the maturation of TDSCs-poly(L-lactide-co- $\epsilon$ -caprolactone)/collagen scaffold constructs for tendon tissue engineering. *Biomaterials* 2014;35:2760–72. doi:10.1016/j.biomaterials.2013.12.042.
- [49] Bosworth LA. Travelling along the Clinical Roadmap: Developing Electrospun Scaffolds for Tendon Repair. *Conf Pap Sci* 2014;2014:1–6. doi:10.1155/2014/304974.
- [50] Mouthuy P-A, Zargar N, Hakimi O, Lostis E, Carr A. Fabrication of continuous electrospun filaments with potential for use as medical fibres. *Biofabrication* 2015;7:25006. doi:10.1088/1758-5090/7/2/025006.
- [51] Laranjeira M, Domingues RMA, Costa-Almeida R, Reis RL, Gomes ME. 3D Mimicry of Native-Tissue-Fiber Architecture Guides Tendon-Derived Cells and Adipose Stem Cells into Artificial Tendon Constructs. *Small* 2017;13:1–13. doi:10.1002/sml.201700689.
- [52] Abhari RE, Mouthuy PA, Vernet A, Schneider JE, Brown CP, Carr AJ. Using an industrial braiding machine to upscale the production and modulate the design of electrospun medical yarns. *Polym Test* 2018;69:188–98. doi:10.1016/j.polymertesting.2018.05.014.
- [53] Tare M. Dental rolls: A suitable model for practising tendon repair techniques. *J Hand Surg Am* 2004;29:506–7. doi:10.1016/j.jhsb.2004.05.006.
- [54] Ingraham JM, Weber RA, Weber RA. Utilizing a simulated tendon to teach tendon repair technique. *Hand* 2009;4:150–5. doi:10.1007/s11552-009-9184-9.

- [55] Abdulal S, Onyekwelu O. An alternative model for teaching tendon repair and surgical skills in plastic surgery. *JPRAS Open* 2016;7:12–5. doi:10.1016/j.jpra.2015.11.003.
- [56] Bosworth LA, Rathbone SR, Bradley RS, Cartmell SH. Dynamic loading of electrospun yarns guides mesenchymal stem cells towards a tendon lineage. *J Mech Behav Biomed Mater* 2014;39:175–83. doi:10.1016/j.jmbbm.2014.07.009.
- [57] Bradley RS, Robinson IK, Yusuf M. 3D X-Ray Nanotomography of Cells Grown on Electrospun Scaffolds. *Macromol Biosci* 2017;17:1–8. doi:10.1002/mabi.201600236.